Supporting Information for

Adsorption at confined interfaces

Prudhvidhar Gaddam[†], Robert Grayson[†], and William Ducker*

[†]these authors contributed equally to the paper

*For correspondence: wducker@vt.edu

Department of Chemical Engineering, Virginia Tech, Blacksburg, VA 24061, USA.

A. Interference Terms

The interference terms for the calculation of Eq 11 are:

$$\Psi_{in}^{||,p} = t_{54}^{||,in} t_{43}^{||,in} (1 - r^{||,in} \mathrm{e}^{\mathrm{i2pd}}) / (1 - r^{||,in} r_{34}^{||,in} \mathrm{e}^{\mathrm{i2p(d+\delta)}})$$

$$\Psi_{in}^{\perp} = t_{54}^{\perp,in} t_{43}^{\perp,in} (1 + r^{\perp,in} \mathrm{e}^{\mathrm{i2pd}}) / (1 - r^{\perp,in} r_{34}^{\perp,in} \mathrm{e}^{\mathrm{i2p(d+\delta)}})$$

$$\Psi_{in}^{||,n} = t_{54}^{||,in} t_{43}^{||,in} (1 + r^{||,in} \mathrm{e}^{\mathrm{i2pd}}) / (1 - r^{||,in} r_{34}^{||,in} \mathrm{e}^{\mathrm{i2p(d+\delta)}})$$

$$\Psi_{out}^{||,p} = t_{45}^{||,out} t_{34}^{||,out} (1 - r^{||,out} \mathrm{e}^{\mathrm{i2qd}}) / (1 - r^{||,out} r_{34}^{||,out} \mathrm{e}^{\mathrm{i2q(d+\delta)}})$$

$$\Psi_{out}^{\perp} = t_{45}^{\perp,out} t_{34}^{\perp,out} (1 + r^{\perp,out} \mathrm{e}^{\mathrm{i2qd}}) / (1 - r^{\perp,out} r_{34}^{\perp,out} \mathrm{e}^{\mathrm{i2q(d+\delta)}})$$

$$\Psi_{out}^{||,n} = t_{45}^{||,out} t_{34}^{||,out} (1 + r^{||,out} \mathrm{e}^{\mathrm{i2qd}}) / (1 - r^{||,out} r_{34}^{||,out} \mathrm{e}^{\mathrm{i2q(d+\delta)}})$$

$$p = 2\pi n_3 / \lambda_{in} \cos \theta_3^{in}$$

$$q = 2\pi n_3 / \lambda_{out} \cos \theta_3^{out}, \text{ (E1)}$$

where $||$ refers to parallel to the plane of incidence and $\perp$ refers to perpendicular to the plane of incidence. The superscripts p and n denote parallel to the interface and normal to the interface, respectively. $t_{ij}^{\perp,in}$ is the Fresnel coefficient of transmission for an illuminating light wave crossing from the ith to the jth layer (Fig. 3) at an angle of incidence ϑ_i^{in}, and wavelength λ_{in}. Similarly the coefficient $r_{ij}^{||,out}$ is the Fresnel coefficient of reflection for an emitted light wave crossing from the ith to the jth layer with an angle of incidence ϑ_i^{out}, and wavelength λ_{out}.

B. Figures

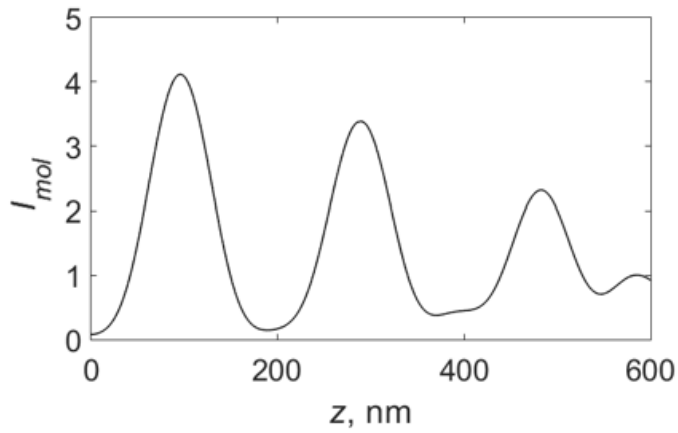

S1. Intensity of fluorescein fluorescence emission as a function of position within the crack, *z*, with *D* = 600 and t = 0. The interference is dominated by the silicon interface such that the shape of this curve is nearly invariant as *D* changes. For greater *D* the curve is extended along the horizontal axis; for smaller *D* reduced. For small *t*, the curve is shifted left by approximately *t*.

If we wish to minimize changes in emission intensity as a function of z, it is best to have the fluid gap situated near a maximum or minimum. If we wish to minimize the z gradient of $I_j(z) + I_j(D - z)$, the fluid gap should be at an inflection point.

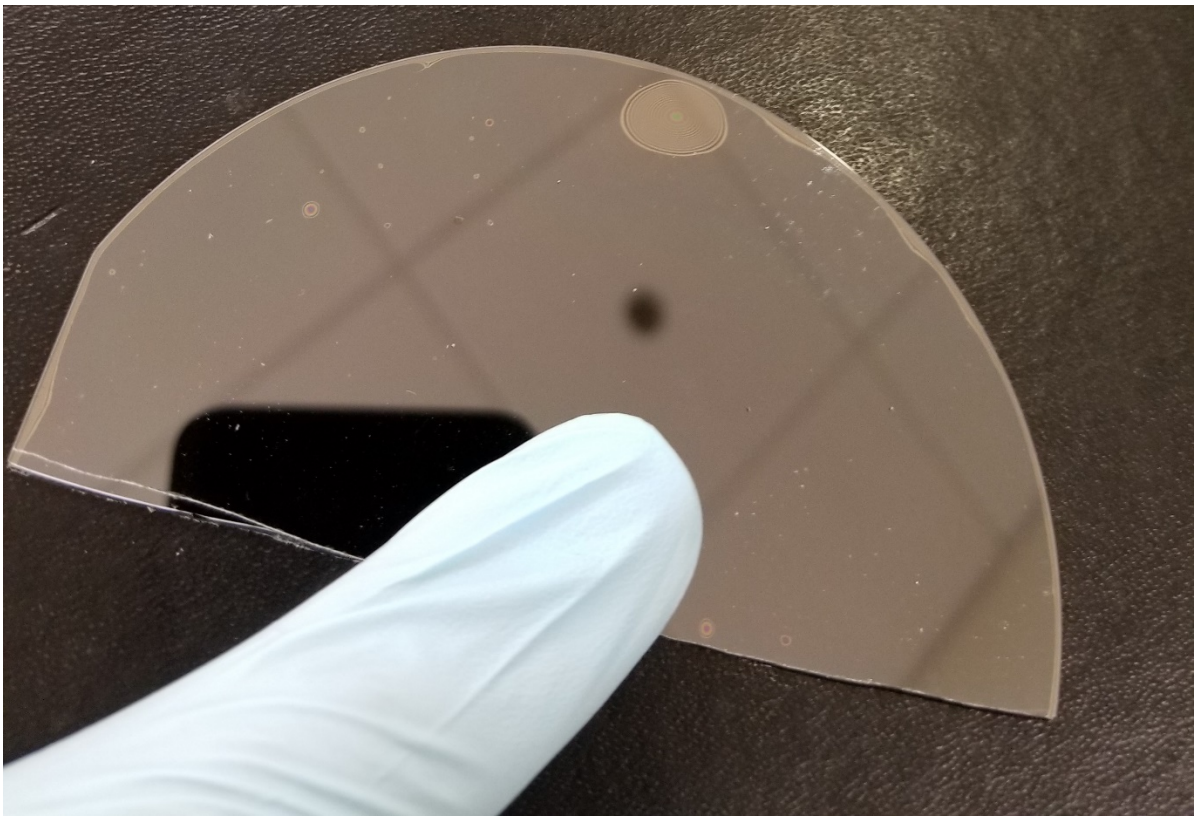

Fig. S2. Photograph of the dual wafer construct showing the radial crack around the perimeter. The light colored region around the perimeter is the region of the crack.

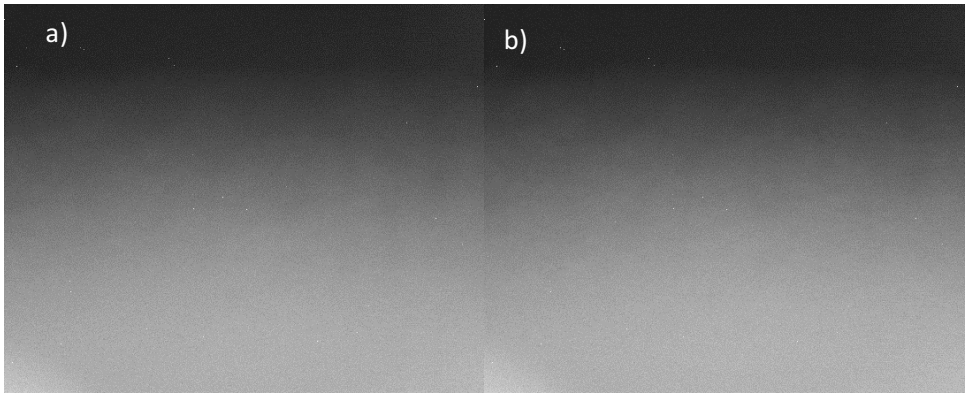

Fig. S3. Optical images of crack spaced 5 minutes apart in time. The lack of change in intensity is consistent with no change to the concentration of fluorescein in the thin film.

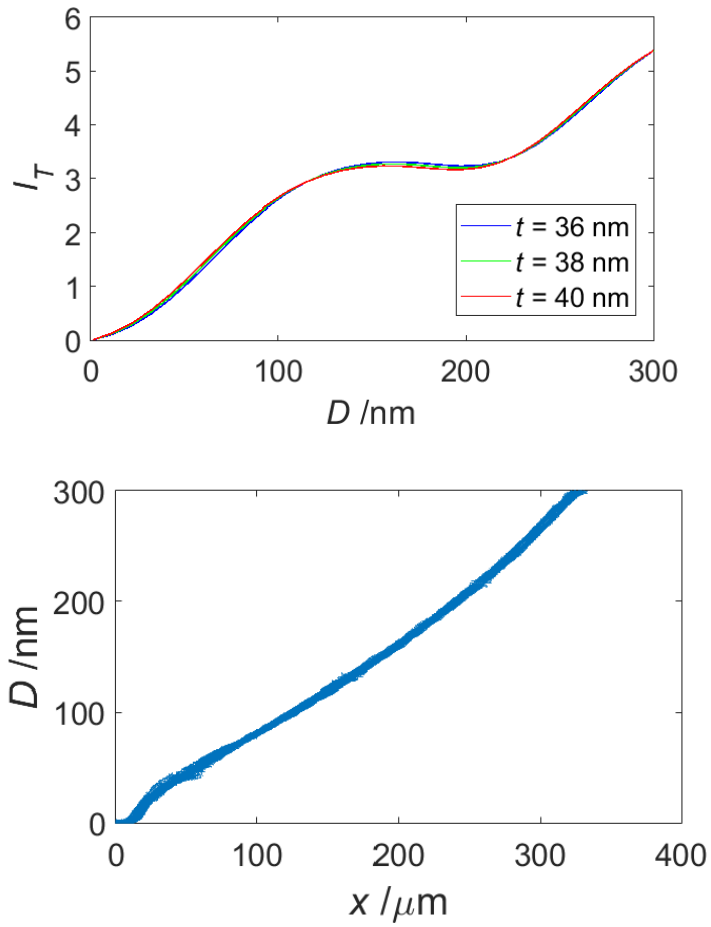

Fig. S4 Top: Intensity vs separation calculated from the model for various oxide thicknesses. Over this range of *D*, small variations in *t* cause small changes in the curvature of the *I* vs *D* curve. **Bottom**: Crack profile. Every pixel (~200,000) where *D*>0 is represented by a point in the figure. *x* is the distance perpendicular to a line fitted to the crack tip.

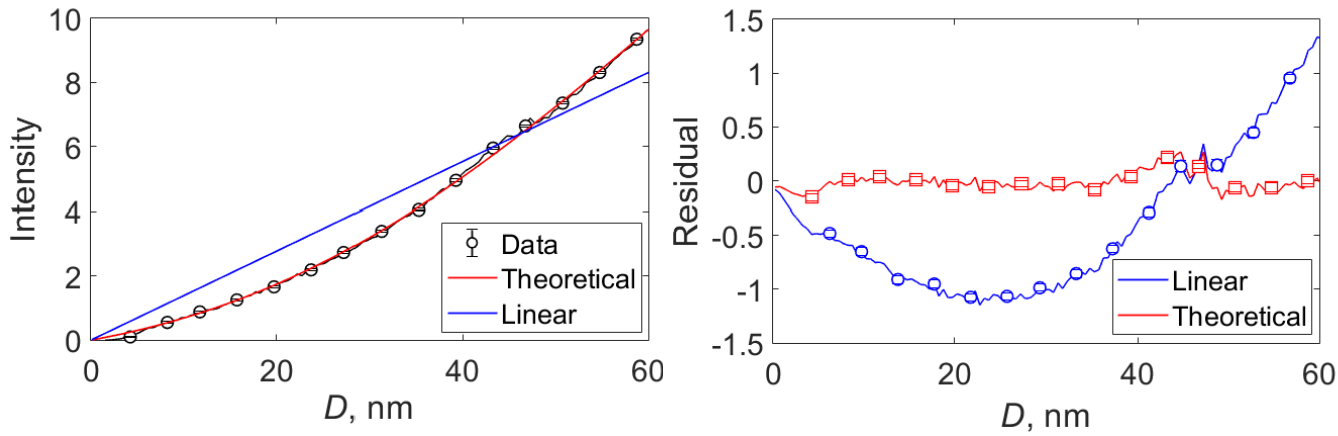

Fig S5. Left: Fluorescence emission intensity over a range of 0–60 nm for κ^{-1} = 0.50 nm solution and a model assuming uniform molecular distribution. Plotted data are the average of intensities binned for a 0.5 nm range around each shown *D*. Error bars represent standard error of the same binned data. An oxide thickness of 36.8 nm was determined from interferometry of the sample, and used in the model. Two fits to the data are shown: (1) the optical model fit and (2) a linear fit. The optical model has one parameter, the magnitude, and the linear fit has a fitted slope with the fit restrained to pass through the origin. The range of the fit is 20 < D < 60 nm. Right: Residuals for the optical model and the linear fit. The optical model agrees very well with the data, even for D < 20 nm. Clearly the optical model is a better fit, so the nonlinearity of *I* vs *D* is not negligible.

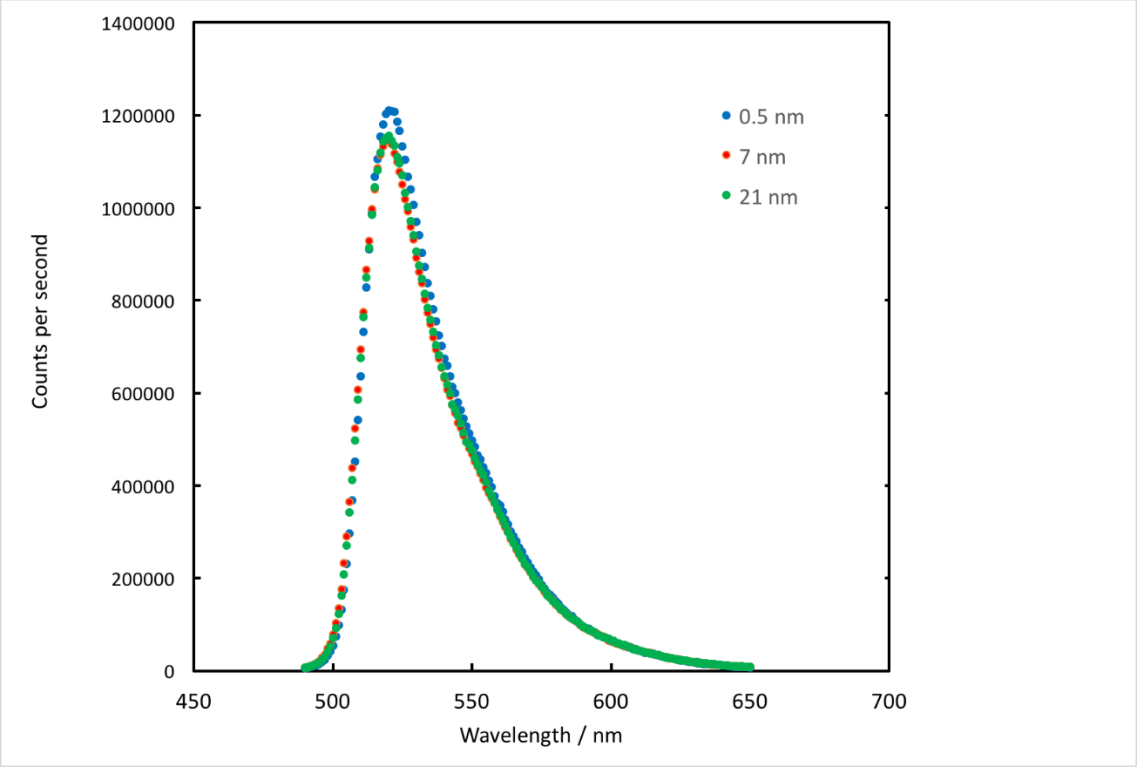

Fig. S6. Emission of 67 µM aqueous fluorescein solution as a function of Debye-length in NaCl solution. The emission filter range in the microscopy was 525±25 nm. The integral over the range 500–550 nm deviates by 7% or less for 7 nm or 21 nm compared to the 0.5 nm solution and was not found significant in a Student's t-test.

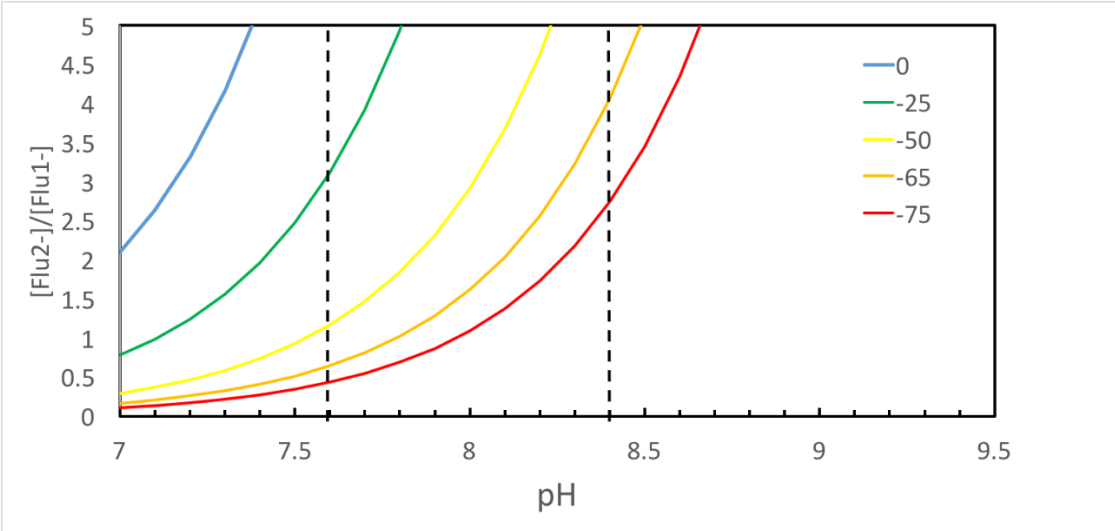

Fig. S7: Ratio of dianion to monoanion as a function of pH calculated from Eq 18 as a function of the potential. The calculation was done for pK'= 6.68, which is the activity-corrected pK for the κ^{-1} = 14 nm and 21 nm solution. The ratio increases slightly for shorter Debye-lengths. E.g. at 50 mV, the ratio is given the following table:

κ^{-1}	pH	
nm	7.6	8.4
0.5	3	17.6
4	1.4	8.6
7	1.2	7.7
14	1.2	7.3
21	1.2	7.3

C. Details of Analysis for Optical Measurements:

Interferometry:

Optical images are background-corrected using a separate image with no features in the field of view. The background image is smoothed using a moving average, on which each smoothed pixel value is the average of a square grid of pixels around it. The smoothed background intensity data is subtracted from the interferometry picture. Near the perimeter of the image there are not enough pixels to compute the average for a grid of the desired size. Pixels where this is the case are excluded from the analysis.

The oxide thickness was measured using interferometry. The oxide thickness controls the interference at the crack tip such that it can be determined from the pixel intensity as $D \rightarrow 0$. In practice, identifying the crack tip in the image can be difficult due to noise. In most cases we found that the intensity at $D = 0$, i.e. where the glass and oxide are directly bonded, was not independent of position; it increased as a function of x-distance from the crack tip. The intensity as the crack begins to open is known from calculation to increase as a function of x-distance from the crack tip. Thus the intensity passes through a minimum moving from the bonded section to the opening of the crack. The location of the minimum in intensity was regarded at the crack tip in our analysis. We estimate that the there is an error of about 2 nm in determining $D = 0$.

Calculating D using the interference pattern involves inverting a squared cosine. The inverse becomes very steep at the limits of its domain, -1 and 1. This means that the measurement of D becomes very sensitive to noise in pixel intensity near points of total constructive and destructive interference. In order to mitigate this issue we smooth over a larger range of pixels near these points. To reduce noise in the interferometry data, we smooth the entire array of pixel intensities using a moving average. The span of the average, i.e. the size of the pixel grid averaged for each point, grows as a function of the gradient in intensity such that it is maximized at intensity maxima and minima (zero gradient) and minimized between. For example, the grid was 13×13 pixels (about 9 µm wide) at the maximum and 5×5 pixels (about 3.5 µm wide) at the inflection. In the proximity of the crack tip we make an exception to this rule and use minimal smoothing (5×5 pixels) so as not to bias the position of this intensity minimum.

Fluorescence:

The background correction for the fluorescence images is the same as for the interferometry images. The fluorescent intensity data is not smoothed.

Intensity vs Separation:

A separation is computed for each pixel in the interferometry image (where there is a crack) and is mapped to the corresponding pixel in the fluorescence image to give fluorescent intensity as a function of separation. The intensity values are corrected to be zero in the limit of $D \rightarrow 0$ by subtracting the average of the 100 lowest D data points where $D > 0$. These 100 data points spanned a range of less than 0.1 nm.

Table S1. Refractive indices of layers

Layer	Material	*n*, interferometry (λ=445nm)	*n*, excitation (λ=470nm)	*n*, emission (λ=525nm)
1	Air	1.00028[1]	1.00028[1]	1.00028[1]
2	Glass	1.479[2]	1.477[2]	1.474[2]
3	Water	1.337[3]	1.336[3]	1.334[3]
4	SiO_2 (thermal)	1.469[†4]	1.469[†4]	1.469[†4]
5	Silicon	4.753+0.163*i**[5]	4.503+0.108*i***[5]	4.185+0.056*i****[5]

† at 546.1 nm

* averaged over 445 ± 25 nm

** averaged over 470 ± 20 nm

*** averaged over 525 ± 25 nm

References

1. Section 10 Index of Refraction of Air. In *CRC Handbook of Chemistry and Physics 98th Edition (Internet Version 2018)* Rumble, J. R., Ed. CRC Press/Taylor & Francis: Boca Raton, FL, 2018.
2. BOROFLOAT® 33 – Optical Properties. http://www.schott.com/d/borofloat/bde16ad3-70e5-48a0-b8ac-9146fcd34511/1.0/borofloat33_opt_en_web.pdf (accessed March 16, 2018).
3. Hale, G. M.; Querry, M. R., Optical constants of water in the 200-nm to 200-µm wavelength region. *Applied optics* **1973,** *12* (3), 555-563.
4. Taft, E.; Cordes, L., Optical Evidence for a Silicon-Silicon Oxide Interlayer. *Journal of The Electrochemical Society* **1979,** *126* (1), 131-134.
5. Section 12 Optical Properties of Selected Elements. In *CRC Handbook of Chemistry and Physics 98th Edition (Internet Version 2018)* Rumble, J. R., Ed. CRC Press/Taylor & Francis: Boca Raton, FL, 2018.